HHS Public Access

Author manuscript

Nat Neurosci. Author manuscript; available in PMC 2014 August 01.

Published in final edited form as:

Nat Neurosci. 2014 February ; 17(2): 269–279. doi:10.1038/nn.3614.

Cell type-specific genetic and optogenetic tools reveal novel hippocampal CA2 circuits

Keigo Kohara[1,*], **Michele Pignatelli**[1,*], **Alexander J. Rivest**[1], **Hae-Yoon Jung**[1], **Takashi Kitamura**[1], **Junghyup Suh**[1], **Dominic Frank**[1], **Koichiro Kajikawa**[1], **Nathan Mise**[2,†], **Yuichi Obata**[2], **Ian R. Wickersham**[3], and **Susumu Tonegawa**[1,4]

[1]RIKEN-MIT Center for Neural Circuit Genetics at the Picower Institute for Learning and Memory, Department of Biology and Department of Brain and Cognitive Sciences, Massachusetts Institute of Technology, Cambridge, Massachusetts 02139, USA

[2]RIKEN BioResource Center, 3-1-1 Koyadai, Tsukuba, Ibaraki 305-0074, Japan

[3]Media Lab, Massachusetts Institute of Technology, Cambridge, Massachusetts 02139, USA

[4]Howard Hughes Medical Institute, Massachusetts Institute of Technology, Cambridge, MA 02139, USA

Abstract

The formation and recall of episodic memory requires precise information processing by the entorhinal-hippocampal network. For several decades, the trisynaptic circuit, entorhinal cortex layer II (ECII)→dentate gyrus (DG)→CA3→CA1 and the monosynaptic circuit ECIII→CA1 have been considered the main substrates of the network responsible for learning and memory. Circuits linked to another hippocampal region, CA2, have only recently come to light. Here, by using highly cell type-specific transgenic mouse lines, optogenetics, and patch-clamp recordings, we show that DG cells, long believed not to project to CA2, send functional monosynaptic inputs to CA2 pyramidal cells, through abundant longitudinal projections. CA2 innervates CA1 to complete an alternate trisynaptic circuit but, unlike CA3, projects preferentially to the deep rather than superficial sublayer of CA1. Furthermore, contrary to the current knowledge, ECIII does not project to CA2. These new anatomical results will allow for a deeper understanding of the biology of learning and memory.

Correspondence should be addressed to: S.T. (tonegawa@mit.edu).

*These authors contributed equally to this work

†present address: Department of Environmental Preventive Medicine, Jichi Medical University, Tochigi 329-0498, Japan

Author Contributions

K.K. conceived, designed, and performed the anatomical and molecular experiments for the DG-CA2 connections. A.J.R conceived, designed, and performed the anatomical and molecular experiments for the EC-CA2 connections. M.P., K.K., and A.J.R. designed the optogenetic experiments. M.P. performed the electrophysiological experiments and the analysis. H.J. conducted the electrophysiological experiments in the early phase of the project. J.S. participated in the early phase of the anatomical experiments. D.F. and K. Kajikawa performed most of the injections. T.K. generated AAV-TRE-ArchT-GFP. K.K. generated the CA2 mouse line. N.M. and Y.O. generated the DG mouse line. I.R.W. provided the rabies virus and associated methods. K.K., M.P., A.J.R, and S.T. wrote the manuscript. S.T. supervised the entire project.

The authors declare no competing financial interests.

Keywords

hippocampus; trisynaptic circuit; CA2; dentate gyrus (DG); mossy fibers (MFs); granule cells (GC); entorhinal cortex (EC); CA1 sublayers; optogenetics; Cre transgenic mice; neural circuit genetics; rabies virus

The hippocampus plays a cardinal role in the acquisition and recall of episodic memory[1]. For several decades[2], the trisynaptic circuit, entorhinal cortex layer II (ECII)→dentate gyrus (DG)→CA3→CA1, has provided the anatomical substrate for memory circuit functions such as pattern separation and pattern completion as demonstrated by both modeling[3] and experimentation[4–7]. The hippocampus, however, includes an additional subregion named CA2[8]. The CA2 region is classically defined as the area located between the CA3 and the CA1 regions with large pyramidal cells that, in contrast to CA3 cells, lack "thorny excrescences" (complex spines) on the apical dendrites, and lack innervation from the DG[8, 9]. An additional classical criterion for the CA2 region is strong hypothalamic afferents from the supramammillary nucleus (SUM)[9–11]. Recent electrophysiological studies proposed CA2 as the relay of a potent monosynaptic pathway, receiving strong afferents from both ECII and ECIII and innervating CA1 pyramidal cells[12, 13]. In addition to the monosynaptic inputs provided by the perforant and temporoammonic paths, CA2 receives a direct input from CA3[13, 14]. Synaptic transmissions at the ECIII-CA2 and ECII-CA2 connections are strong and highly plastic[13], whereas at the CA3-CA2 synapses connections are dominated by feedforward inhibition[13] and are resistant to long term potentiation[14, 15].

The CA2 region has been known to expresses multiple region-specific genes[15–17] and a recent study using in situ hybridization proposed a redefinition of the CA2 region which is substantially wider than previously thought[18]. However, the relationship between the putative CA2 region newly proposed by molecular markers and that classically defined by cellular and anatomical criteria has remained unclear. Furthermore, the current knowledge about the afferents and efferents of CA2 is based on electrophysiological stimulation of axons bundles and/or dye injections into the source or target areas in which the specificity is potentially compromised. Defining this underexplored hippocampal region more extensively and establishing its connections more precisely are crucial for our understanding of the hippocampus, the brain system that plays a pivotal role in episodic learning and memory[1].

In this study, by using cell type-specific methods of high resolution, we first investigated the relationships between the new molecularly defined CA2 region and its classic anatomical criteria. In doing so, we revealed a major unsuspected projection from dentate granule cells to CA2 pyramidal cells (DG-CA2) that extend mainly along the longitudinal axis of the hippocampus. Second, we demonstrated, contrary to previous reports[13, 15–17, 19], that ECIII cells do not project directly to CA2 pyramidal cells in any significant way. Third, by exploring the CA2 cell efferents, we found a differential innervation of CA2 pyramidal cells to deep and superficial sublayers of CA1 pyramidal cells. These findings force a major revision to the projection pattern of the entorhinal-hippocampal network for episodic memory.

RESULTS

Molecular, cellular, anatomical and electrophysiological definition of the CA2 region

The putative CA2 marker genes (RGS14[20], PCP4[18] and STEP[21]) were highly coexpressed in the putative CA2 pyramidal cells (PCP4/RGS14 98%±1, STEP/RGS14 100%, PCP4/STEP 98%±1, n=6 mice, Fig. 1a–h). The expression of RGS14 did not overlap with that of the CA1 marker gene, WFS1[22], nor of a transgenic CA3 marker[4] (Supplementary Fig. 1). PCP4-positive CA2 cells did not express GAD67 but expressed CaMKIIα indicating the excitatory nature of these cells (Supplementary Fig. 2). Furthermore, most of the PCP4-positive cells were also positive with α-actinin2, a marker employed by another recent work[13] to help identify CA2 cells (Supplementary Fig. 3). We visualized the dendrites of CA2 neurons with diolistic labeling and found that none of the RGS14-positive neurons had complex spines, but only had simple spines in the stratum lucidum (43 out of 43 RGS14-positive neurons without complex spines, n=4 mice, Fig. 1i–k) in an agreement with the classical criterion for CA2 cells[9]. By contrast, most of the RGS14-negative CA3 neurons had complex spines on their dendrites (29 of 30 RGS14-negative neurons had complex spines, n=4 mice, Fig. 1l) as reported previously[9, 23]. We also injected an anterograde axonal tracer, biotinylated dextran amine (BDA) into SUM and examined the projection pattern from SUM to the hippocampus. We found that BDA-positive SUM projections overlapped with DG granule cells (DGGCs) as shown previously[9–11], and mostly with PCP4-positive CA2 cells (n=3 mice, Fig. 1m–p) satisfying another classical criterion of CA2 cells[9–11]. The RGS14-positive putative CA2 pyramidal cells exhibited intrinsic electrophysiological properties such as: resting membrane potential −70±1 mV, 78±6 MΩ input resistance, 27±1 ms membrane time constant, −44±1 mV action potential threshold, 1±0.2 mV sag amplitude, and a persistent depolarization in response to somatic injection of positive current steps near the action potential threshold. These electrophysiological properties of RGS14-positive pyramidal cells were shared by the α-actinin2-positive CA2 cells[13] and distinguish them from RGS14-negative CA3 and CA1 pyramidal cells (Fig. 1q–t and Supplementary Fig. 4). There was no evidence of heterogeneity in these properties along the ~300 μm-wide band of RGS14-positive cells (Supplementary Fig. 4). Furthermore, CA2 cells defined by RGS14 seem to have similar soma sizes (average soma surface 309±30 μm^2) and dendritic morphology to those defined by α-actinin2[13] (Supplementary Fig. 4). We have thus shown that cells expressing the molecular markers for CA2 satisfy classical criteria with respect to both their dendritic spine morphology and projections from the SUM[8–11], as well as more recently reported criteria of their intrinsic electrophysiological properties[13].

Dentate mossy fibers innervate CA2 pyramidal cells

We then examined by immunohistochemistry and viral tracing whether the newly defined CA2 pyramidal cells lack mossy fiber (MF) innervation, another classical criterion of CA2 cells[8, 9]. To our surprise, we found that calbindin-positive MFs[24] projected extensively to PCP4-positive CA2 neurons in the stratum lucidum (the percentage of PCP4-postive cells overlapping with MFs: MF+ 82.2±1.1%; that of non-overlapping with MFs: MF− 17.8±1.1%, n=5 mice, Fig. 2a,b, Supplementary Fig. 5 and 6). Next, we examined the distribution of ZnT3[25], a presynaptic vesicle marker of MFs, and VGluT1, a glutamatergic presynaptic vesicle marker, in the stratum lucidum of CA2. We found that ZnT3 and

VGluT1 double positive presynaptic clusters were located on RGS14-positive dendrites (Fig. 2c,d). Furthermore, we found that ZnT3 clusters overlapped with a postsynaptic marker, PSD95 on RGS14-positive dendrites (Fig. 2e–h). These data suggest that contrary to the classical definition[8, 9], MFs form synaptic contacts with CA2 pyramidal neurons. We examined the morphology of MF terminals by infecting DG with HSV mini-enk promoter-ChETA-YFP (Fig. 2i) and found that CA2 received small MF boutons in contrast to the giant MF boutons received by CA3[9] (average bouton diameters: CA2 0.97±0.05 μm, n=60 boutons; CA3 2.11±0.1 μm, n=43 boutons; from n=5 mice, *KS*<0.001, Fig. 2j–l).

The longitudinal component of MFs projects mostly within the CA2 region

MFs are known to extend both transversally within a lamella and longitudinally in the septotemporal direction[26]. However, the longitudinal component has been thought to run exclusively within CA3[9, 26–28]. To reinvestigate this issue, we visualized axonal projections from a limited population of DGGCs by injecting Cre-dependent tTA lentivirus and adeno-associated virus (AAV9-TRE-ArchT-GFP) into the dorsal DG of a novel DGGC-specific Cre transgenic mouse (Dock10 Cre, Supplementary Fig. 7, Fig. 3a). We found that while MFs projected mainly in the transverse plane in CA3, they abundantly projected longitudinally in CA2 for as long as ~2 mm (Fig. 3b–e). To determine the extent and the direction of the longitudinal projection of MFs within CA2, we applied the same approach but infected only dorsal, intermediate or ventral DG (n=3 mice per group). Results indicate: 1) MFs from dorsal DGGC extend to dorsal and intermediate CA2 but not to ventral CA2 (Fig. 3f,i,l,o), 2) MFs from intermediate DGGC extend to intermediate and ventral CA2 but not to dorsal CA2 (Fig. 3g,j,m,p), 3) MFs from ventral DGGC do not extend to dorsal or intermediate CA2 (Fig. 3h,k,n,q). These results indicate that the longitudinal component of MFs projects exclusively in the septotemporal direction. Analysis of the MF terminal distribution confirmed that the septotemporal longitudinal component of MFs mostly innervates the CA2 region, although, a small fraction of the very distal CA3 region, adjacent to CA2, also received scattered innervations (percent of MF terminals: in CA2 = 90%, in CA3 = 10%; n=680 MF terminals from n=6 mice, two-tailed paired t-test *P*<0.05).

Mossy fibers establish functional monosynaptic connections with CA2 pyramidal cells

We then examined whether DGGCs and CA2 pyramidal cells are functionally connected. For this purpose, we infected DGGC-specific Cre mice with a Cre-dependent adeno-associated virus carrying channelrhodopsin2-YFP[29] (AAV9-EF1α-DIO-ChR2-YFP) to allow for DGGC-specific expression of ChR2-YFP (Fig. 4a–c, Supplementary Fig. 7). Optogenetic stimulation of ChR2-YFP-positive MFs during patch-clamp recording from RGS14-positive CA2 pyramidal cells revealed a reliable excitatory synaptic current (average EPSC amplitude −122±33 pA, n=23, Fig. 4d–f). The EPSCs were sensitive to ionotropic glutamate receptor antagonists (NBQX 10 μM, AP5 100 μM, n=5) and to the antagonist of type II metabotropic glutamate receptors (DCG-IV 1 μM, n=5), a known blocker of MF synaptic transmission[13, 30] (Fig. 4g). Bath application of GABA receptor antagonists did not abolish the synaptic response (GBZ 10 μM, CGP 2 μM, average EPSP amplitude in control 6±1.9 mV, in GBZ/CGP 7.2±2 mV, n=8). To test whether the DG-CA2 connection was monosynaptic, we stimulated MFs optogenetically and directly compared the onset of CA1, CA2, and CA3 pyramidal cell EPSCs in the same hippocampal slices. CA2 responses

displayed a rapid onset comparable to those of CA3 whereas CA1 responses displayed a delayed onset accountable to polysynaptic connection (average EPSC onset: CA1 7.04±0.48 ms, CA2 2.02±0.13 ms and CA3 1.58±0.07 ms, n=9 triplets, Fig. 4h–j). In addition, the onset of the CA2 response always preceded the occurrence of the first action potential peak elicited in CA3 cells through MF activation, excluding the possibility that CA2 EPSCs were mediated by polysynaptic connection from CA3 cells (CA3 firing probability 0.36±0.04, n=20 trials per cell; average action potential peak time 3.85±0.34 ms, n=14 CA3 pyramidal cells, Supplementary Fig. 8). These results demonstrated a functional and direct excitatory monosynaptic connection from DGGCs to CA2 pyramidal cells and reinforced our anatomical observations (Fig. 2).

Impact and modulation of the DG-CA2 connection

Optogenetic stimulation of MFs with a single light pulse combined with recordings of CA2 pyramidal cells in current mode revealed spiking activity in 22% of the cells (5 out of 23). However, a 30 Hz train of 15 light pulses revealed spiking activity in 61% of the cells (14 out of 23). Spike probability in response to the first pulse was 0.23±0.1 (20 trials per cell, n=23), and doubled during the next train pulses with a spike probability of 0.43±0.2 in response to a recovery pulse delivered 500 ms after the train (Fig. 5a–d). These results suggest dynamics ruled by synaptic facilitation. Analysis of the excitatory postsynaptic potential (EPSP) in response to single light pulse revealed a large EPSP (average EPSP amplitude 4.7±0.8 mV, n=24) followed by inhibition (Fig. 5e). Inhibition was primarily sensitive to a GABAb receptor antagonist (CPG 2 μM), and application of a GABAa antagonist (GBZ 50 μM) revealed a fast inhibitory response overlapping with the excitatory one (Fig. 5f,g). These results indicate the presence of feedforward inhibition elicited by MF activation. CA2 pyramidal cells are known to be locally controlled by CA2 interneurons[31] and the feedforward inhibition could be mediated by these interneurons. Indeed, optogenetic stimulation of MFs with a single light pulse elicited spiking activity in 46% (5 out of 11, average firing probability 0.56±18) of CA2 interneurons recorded in current mode (Fig. 5h,i). Analysis of the first action potential peak time confirmed the possibility of a fast feedforward inhibitory circuit (average AP peak time 4.9±0.6 ms, Fig. 5j). When recorded in voltage clamp configuration, all CA2 interneurons responded to optogenetic stimulation of MFs with a large EPSC (average EPSC amplitude −138±88 pA, average EPSC onset 2.3±0.1 ms, n=11, Fig. 5k). CA2 interneurons were identified by biocytin staining, intrinsic electrophysiological properties, and by expression of GAD67 (n=11). Only a fraction of them expressed parvalbumin (n=3). Although both parvalbumin-positive and parvalbumin-negative CA2 interneurons displayed EPSCs in response to optogenetic stimulation of MFs. The recorded CA2 interneurons were located in the stratum oriens (n=2), in the deep stratum pyramidale (n=2) or in the border between lucidum and pyramidale (n=7). These results demonstrate a functional monosynaptic connection between MFs and CA2 interneurons and support the feedforward inhibition observed in the CA2 pyramidal cells in response to optogenetic stimulation of MFs (Fig. 5l). As reported for CA3 interneurons[32], local CA2 interneurons also receive direct projections from DG, constituting a feedforward inhibitory mechanism that could control the output of CA2 pyramidal cells by modulating their rate or by controlling their timing.

Lack of direct projections from ECIII to the CA2 region

It was previously reported that the CA2 region is the convergence point of direct cortico-hippocampal projections from ECII and ECIII[13]. However, this study did not employ an entirely cell or axon type-specific stimulation method. To selectively label MECIII axons with YFP, we injected the AAV9-EF1α-DIO-ChR2-YFP into the EC of MECIII pyramidal cell-specific *pOxr1*-Cre transgenic mice[33] (Fig. 6a). To selectively label MECII projections, we stained hippocampal slices of these mice for netrin-G2, a MECII-specific marker[34]. YFP-positive MECIII cell axons terminated sharply at the proximal end of the calbindin-positive CA1 region and did not enter the RGS14-positive CA2 nor extend to CA3 (Fig. 6a and Supplementary Fig. 9). Consistent with a prior report[35], netrin-G2-positive fibers extended beyond the DG and terminated in the stratum lacunosum-moleculare (SLM) of CA3 and CA2 (Fig. 6a). We considered the possibility that ChR2 may not be expressed sufficiently in some MECIII cells in the transgenic mice infected by the Cre-dependent AAV. Therefore, we injected a non-Cre-dependent and excitatory neuron-specific AAVrh8-CaMKIIα-ChR2-YFP into the EC superficial layers of wild type mice. It is known that ECIII cells, but not ECII cells, innervate the contralateral hippocampus[36, 37]. The contralateral component of ECIII axons did not enter the CA2 region of the wild type mice (Supplementary Fig. 10a–d) Furthermore, when we investigated the cortico-hippocampal projections arising from the lateral entorhinal cortex (LEC), we found no overlap between LECIII fibers and the CA2 region, confirming previous studies[36, 37] (Supplementary Fig. 10e,f).

By using MECIII cell type-specific optogenetic stimulation we investigated the synaptic transmission of MECIII fibers to CA1, CA2 and CA3 pyramidal cells (Fig. 6b). In agreement with our anatomical observation, only CA1 cells displayed an excitatory response (average EPSC amplitude: CA1 −18±3 pA, n=18, CA2 0 pA, n=10, CA3 0 pA, n=8; average EPSC onset: CA1 3.5±0.2 ms, n=18; Fig. 6c,d). CA1-EPSCs were sensitive to glutamate receptor antagonists (Supplementary Fig. 11a–c). Neither stronger train pulses (Supplementary Fig. 11d–h) nor stimulation under application of GABA receptor antagonists (Supplementary Fig. 11i–o) revealed a response in CA2. This observation was also confirmed by recording distal CA2 cells (n=5) located in the pyramidal cell layer following the end of the stratum lucidum (Supplementary Fig. 12).

To analyze the ECII-mediated connectivity, we went back to the wild type mice in which we injected a non-Cre-dependent and excitatory neuron-specific virus in the superficial layers of the EC (see above). In these mice, ChR2 is expressed in both MECIII and MECII (Fig. 6e and Supplementary Fig. 13). We then investigated the transmission at the synapses between MECII axons and CA2 or CA3 pyramidal cells (Fig. 6f). Since MECIII projects exclusively to CA1 (Fig. 6a,e and Supplementary Fig. 13), any EPSCs recorded in CA2 or CA3 upon optogenetic stimulation must be elicited by MECII axon activation. CA2 pyramidal cells displayed ~4 times larger EPSCs than CA3 cells, consistent with previous observations[13] (CA1 −20±4 pA, n=10; CA2 −403±14 pA, n=16; CA3 −115±27 pA, n=11; CA2 vs. CA3 unpaired t-test $*P<0.05$; average EPSC onset: CA1 3.3±0.3 ms, n=10, CA2 2.5±0.1 ms, n=16, CA3 2.8±0.1 ms, n=11; Fig. 6f–h and Supplementary Fig. 11m–o). Importantly, EPSC amplitudes recorded in CA1 were comparable (two tailed unpaired t-test $P=0.75$) to

those obtained in CA1 cells from *pOxr1*-Cre mice injected with the Cre-dependent AAV9-EF1α-DIO-ChR2-YFP, consistent with the notion that MECII does not innervate CA1 (Fig. 6h).

Although it is unlikely[33], we could not exclude the possibility that axons from a small population of MECIII excitatory neurons were not labeled by YFP in the *pOxr1* transgenic mice. To exclude this possibility, we applied the rabies virus-based monosynaptic tracing technique[38] to the novel CA2-specific Cre knock-in mouse (MAP3K15 Cre, Fig. 7a,b). Contrary to the previously reported anatomical observations obtained with low cell-type specific retrograde tracers[19], EC cells presynaptic to CA2 pyramidal cells (labeled by mCherry) were detected mostly in MECII and LECII; there were very few in MECIII or LECIII (Fig. 7c–e and Supplementary Fig. 14 and 15).

A preferential connection from CA2 to deep CA1 pyramidal cells establishes a novel trisynaptic circuit: DG-CA2-CA1$_{deep}$

Previous studies using classical anatomical criteria showed that CA2 projects to CA1[8, 9, 21, 39] and forms functional synaptic connections with CA1 pyramidal cells[13]. However, how the newly defined CA2 cells project to the downstream CA1 region remains unclear. We infected the CA2-specific Cre knock-in mouse (MAP3K15 Cre) with a Cre-dependent virus, AAV9-EF1α-DIO-ChR2-YFP (Fig. 8a–c and Supplementary Fig. 16). All ChR2-YFP-positive cells expressed PCP4 confirming the high cell type specificity of the knock-in mouse (PCP4/YFP 97%±0.4, n=3 mice, Supplementary Fig. 16. Consistent with previous observations, CA2 axons traveled mainly in the stratum oriens (Supplementary Fig. 16)[8, 21, 39]. Optogenetic stimulation of ChR2-positive CA2 fibers during patch-clamp recordings from CA1 pyramidal cells revealed an excitatory response (average EPSC amplitude −120±20 pA, average EPSC onset 1.9±0.04 ms, n=28) that was sensitive to ionotropic glutamate receptor antagonists (Fig. 8d–g).

It has recently been shown that the CA1 pyramidal cell layer consists of two sublayers, deep and superficial, which are distinct from each other by molecular markers[40] and by electrophysiological characteristics[41]. We compared the response of CA1 sublayer neurons in the same slices to CA2 stimulation and found that calbindin-negative deep CA1 pyramidal cells displayed an excitatory response stronger than calbindin-positive superficial CA1 cells (average EPSC amplitude: deep CA1 −174±33 pA, superficial CA1 −63±11 pA, n=14 pairs, two-tailed paired t-test $P<0.001$, Fig. 8d–g, average EPSC onset: deep CA1 1.8±0.06 ms, superficial CA1 2±0.05 ms, n=14 pairs). This result was not affected by blockers of GABAergic transmission suggesting that the differential innervation of CA1$_{deep}$ and CA1$_{superficial}$ is mediated exclusively by excitatory synaptic connections (average EPSC amplitude in GBZ/CPG: CA1$_{deep}$ −85±18 pA, CA1$_{superficial}$ −41±14 pA, n=7, two-tailed paired t-test $P<0.05$). By applying the same approach to a CA3-specific Cre mouse[4] we found that unlike CA2, CA3 innervates the two CA1 sublayers with equal strength (average EPSC amplitude: deep CA1 −50±17 pA, superficial CA1 −42±24 pA, n=7 pairs, two-tailed paired t-test $P=0.62$, Supplementary Fig. 17; average EPSC onset: deep CA1 3.6±0.25 ms, superficial CA1 4.4±0.8 ms, n=7 pairs). Thus, we have identified a novel trisynaptic circuit,

DG-CA2-CA1$_{deep}$ (Fig. 8h,i), which runs parallel to the classical trisynaptic circuit, DG-CA3-CA1.

DISCUSSION

In this study, we combined several cell type-specific tools and technologies to define the hippocampal CA2 excitatory neurons and their circuits. The major conclusions are: 1) contrary to the traditionally held view, CA2 pyramidal cells receive direct input from DGGCs, 2) CA2 pyramidal cells do not receive direct input from EC layer III cells, and 3) CA2 pyramidal cells project preferentially to CA1 pyramidal cells in the deep sub layer.

The new definition of the CA2 region

The classical definition distinguishes the CA2 pyramidal cells from the CA3 pyramidal cells by lack of complex spines on the apical dendrites[8], by lack of direct innervations of mossy fibers[8], and by strong hypothalamic afferents from the SUM[10, 11]. CA2 pyramidal cells have also been distinguished from CA1 pyramidal cells by their distinctly larger soma sizes and SUM afferents[8, 11]. More recently, the putative CA2 cells were redefined by the molecular marker, PCP4[18]. However, to what extent these cells satisfy the classical morphological and anatomical criteria have not been rigorously investigated. Indeed, the molecularly defined CA2 region extends into a substantially wider area (~300 μm) compared to the classically defined one (~100 μm)[18] (Supplementary Fig. 5).

In this study, we first demonstrated that the expression of additional molecular markers, RGS14 and STEP, as well as MAP3K15, overlaps with PCP4 expression almost perfectly. We then showed that these molecularly defined pyramidal cells satisfy several classical criteria of CA2 cells: the lack of complex spines, presence of strong SUM afferents and relatively large soma sizes. Furthermore, the putative CA2 pyramidal cells defined by multiple molecular markers were distinguished from CA3 and CA1 pyramidal cells by several intrinsic electrophysiological properties reported more recently[13]. There was no major evidence of heterogeneity along the ~300 μm stretch of the RGS14-positive cells with respect to either spine morphologies (Fig. 1i–k) in the stratum lucidum or intrinsic electrophysiological properties (Fig. 1q–t and Supplementary Fig. 4).

The major deviations of the newly defined CA2 region from the classically defined one are 1) direct innervation by mossy fibers (see the following section of the Discussion) and 2) the greater width along the proxi-distal axis in the CA arc. We believe that these differences were revealed by our use of tools and technologies that permit higher levels of cell-type specific analysis at both presynaptic and postsynaptic sides, which were not available when the CA2 region was classically defined. We believe that the new definition of CA2 is more useful for future studies because the cells of the new definition share common molecular, cellular, physiological, and anatomical properties that distinguish them from the cells in the adjacent CA3 and CA1 regions.

A novel trisynaptic circuit, ECII→DG→CA2→CA1$_{deep}$

CA2 is innervated by small MF boutons contacting the shaft and simple spines of the apical dendrites (Fig. 2 and Supplementary. Fig. 18). On the other hand, CA3 receives MF

innervation on both the apical and basal dendrites where giant boutons form synapses with the complex spines of CA3 neurons[9]. This distinction is translated into the greater response amplitude displayed by CA3 neurons upon MF stimulation (average EPSC amplitude: CA2 −66 ± 19 pA, CA3 −939 ± 217 pA, n=9 pairs recorded in the same slices, two-tailed paired t-test $P<0.005$). However, the synapses formed by giant boutons and complex spines represent a unique case in the central nervous system with an unusual synaptic transmission strength[42]. On dendrites, proximal synapses generally have a greater impact on neuronal activity than distal synapses[9]. Indeed, by using optogenetic stimulation of the Schaffer collaterals in the CA3-specific Cre transgenic mouse, we demonstrated that the DG-CA2 connection is stronger than that of the CA3-CA2 connection located on a more distal part of the apical dendrite (average EPSC amplitude: DG-CA2 −122 ± 33 pA, n=23; CA3-CA2 −40 ± 33 pA, n=10; two-tailed unpaired t-test $P<0.05$, Supplementary Fig. 19). Furthermore, the DG-CA2 connection is stronger than some other connections within the cortico-hippocampal network such as ECIII to CA1[13] and young GC to CA3[30], two connections known for their behavioral impact[7, 33]. Thus, it is likely that the newly found DG-CA2 connection will also have a significant behavioral impact, although at the moment, it is only a matter of speculation as to the specific function of these connections.

One striking finding about the DG-CA2 connections concerns the extensive longitudinal transfer of information along the septotemporal axis of the hippocampus. Previous studies showed that MFs consist of both transverse and longitudinal projections, the latter running exclusively along the septotemporal direction[26, 27]. Because CA2 has been excluded by definition from the targets of MFs, the CA3 region, particularly the distal part known as CA3a[28], was considered to be the exclusive target of these longitudinal projections. With the new definition of the CA2 region, we have now shown that MFs enter the CA2 region and proceed septotemporally within this region for a long distance (~2 mm, Fig. 3). While 90% of the axonal boutons belonging to the longitudinal component are detected in the stratum lucidum of the CA2 region, only 10% can be detected in the CA3a region, adjacent to CA2. In addition, it has been reported that CA2 axons run septotemporally in the downstream CA1 region[21, 39]. Therefore, CA2 cells appear to be at the center of a septotemporal circuit covering the whole longitudinal axis of the hippocampus. Through the extensive longitudinal projections of MFs and CA2 axons, the novel trisynaptic circuit could provide a substrate for a hierarchical association of information across hippocampal lamellae in contrast to the classical trisynaptic circuit that operates mainly with transverse projections[9]. For example, activation of dorsal DG could easily recruit intermediate CA2 cells, which could have a direct impact on a more ventral CA1 cells, thus establishing a direct link between dorsal and ventral hippocampus and providing a fast route to directly influence downstream regions connected to ventral CA1, such as prefrontal cortex and basolateral amygdala[43].

The novel CA2-linked trisynaptic circuit, ECII→DG→CA2→CA1 also differs from the classical one in the downstream of CA2/CA3. A previous study reported that the functional innervation of CA1 cells provided by CA2 cells is stronger than the one provided by CA3 cells[13]. However, this study did not distinguish between the deep and superficial sublayers of CA1[40]. CA2 axons are known to run preferentially in the stratum oriens[8, 21, 39], where

both the extent of arborization of the basal dendrites and the spine numbers are greater for deep rather than superficial CA1 cells[44, 45]. Consistent with the projection pattern of CA2 axons and with the dendritic morphology of CA1 cells, we demonstrated that the functional synaptic connections made by CA2 cells are about two and a half fold stronger with the deep rather than superficial CA1 cells (Fig. 8). In contrast, Schaffer collaterals of CA3 cells functionally innervated the apical dendrites of both CA1 sublayers with equal strength (Supplementary Fig. 17). The CA2-linked trisynaptic circuit can exert a powerful downstream effect *in vivo* through the higher firing and bursting rates of the deep layer CA1 pyramidal cells[41]. Although the target of the CA1 sublayers is yet to be determined, it is possible that the information conveyed by the two trisynaptic circuits is directed to differential targets and thereby used for distinct functions.

Significantly, the two trisynaptic circuits are not entirely independent as they interact mutually between CA3 and CA2. The CA3-CA2 connections[46] are known to be dominated by feedforward inhibition[13]. By combining optogenetic stimulation of ChR2-YFP-positive CA2 fibers and patch-clamp recordings from CA3 pyramidal cells, we show that CA2-CA3 connections are also dominated by inhibition (Supplementary Fig. 19). This mutually inhibitory loop of the connections between CA2 and CA3 suggests a competitive relationship between the two trisynaptic circuits.

CA2 pyramidal cells do not receive direct input from ECIII pyramidal cells

We have shown this by three methods, all with high cell type-specificity. First, YFP-labeled axons from MECIII-specific transgenic Cre mice did not overlap with RGS14-positive CA2 cells (Fig. 6). Second, MECIII cell-specific optogenetic stimulation (Fig. 6), even with train of light pulses (Supplementary Fig. 11 and 12) or in the presence of GABA receptor antagonists (Supplementary Fig. 11), did not reveal any response in CA2 cells (Supplementary Fig. 11 and 12). Third, the rabies virus-based monosynaptic tracing technique conducted with CA2 pyramidal cell-specific Cre knock-in mice revealed only a few positive cells in MECIII or LECIII that may project to CA2 pyramidal cells (Fig. 7).

We did consider the possibility that the *Oxr1* promoter used for the generation of MECIII-specific transgenic mice is not active in some MECIII cells, and that axons of these cells may reach the CA2 region and activate their pyramidal cells. However, the lack of any detectable overlap between contralateral ECIII cell axons and RGS14-positive cells in wild type mice makes this possibility highly unlikely (Supplementary Fig. 10). These data are at odds with those of an influential study by Chevaleyre and Siegelbaum[13] who found that CA2 cells responded robustly to electric stimulation of axons in SLM. It is highly unlikely that electric stimulation of axons from the very few MECIII or LECIII cells observed by our rabies virus-based retrograde tracing experiment (Fig. 7) could account for the robust synaptic transmission and plasticity that Chevaleyre and Siegelbaum detected. In fact, these few MECIII and LECIII cells may actually be long-range inhibitory neurons which are known to project to the hippocampus[47].

Could it be possible that they and we have recorded from two different sets of cells? Chevaleyre and Siegelbaum recorded from α-actinin2-positive large pyramidal cells “located in the area following the end of the mossy fiber tract” (see Supplementary Fig. 4

and page 570 of reference 14). In this area, virtually all α-actinin2-positive cells are also PCP4-positive (Supplementary Fig. 3). These PCP4-positive cells share with the rest of PCP4-positive cells the physiological properties characteristic of CA2 cells (Supplementary Fig. 4). But we failed in inducing EPSCs from these distal CA2 cells, even with strong optogenetic stimulation of ChR2-positive axons of MECIII cells (Supplementary Fig. 12). In addition, recordings of very proximal CA1 pyramidal cells in response to optogenetic stimulation of MECIII fibers revealed only weak responses, typical of more distal CA1 cells (Supplementary Fig. 11). Despite all these data and reasoning, one cannot exclude the possibility that Chevaleyre and Siegelbaum recorded from a subpopulation of cells, which we did not cover in our CA2 recording experiments.

Could it be possible that the axons stimulated by the two studies are not entirely the same? Unlike our approach aided by the cell type-specific genetic method, Chevaleyre and Siegelbaum employed electric stimulation of axonal bundles in the temporo-ammonic (TA) pathway. This leaves a possibility open that fibers other than those from MECIII could also have been recruited[9]. It is even possible that the electricity spilled out to nearby ECII cell fibers (within ~60 μm), which run through the distal molecular layer of the DG and are known to be a robust source of stimulation for CA2 pyramidal cells[13] (Figure 6). This latter possibility (i.e. electricity spillage) is suggested by their observation that CA3a cells also responded substantially to the same stimulation of axon bundles in the TA pathway. These connections were also reported in earlier studies conducted with similar methods[48, 49]. However our cell type-specific axonal tracing and optogenetic stimulation experiments demonstrated that ECIII cells do not innervate CA3 cells (Fig. 6) suggesting that there may have been electricity spillage in Chevaleyre and Siegelbaum's experiment. Nevertheless, it is difficult to be certain that the conflicting results obtained stem from activation of different set of axons in their and our studies.

In contrast to the lack of a CA2 response to ECIII axon stimulations, we confirmed Chevaleyre and Siegelbaum's finding[13] that CA2 pyramidal cells respond robustly to the stimulation of axons from ECII stellate cells (Fig. 6f–h). What emerges from all these data are two mutually exclusive direct hippocampal projection patterns of ECIII→CA1 and ECII→DG/CA3/CA2.

Possible functions of the various circuits in the entorhinal-hippocampal network

The classical trisynaptic circuit has been a fertile ground to which genetic manipulations targeted to specific subregions and connections thereof were applied to investigate their casual roles in specific aspects of entorhinal-hippocampal learning and memory such as pattern separation and pattern completion[4–7]. In contrast, studies relevant to the role of the novel trisynaptic circuit linked to CA2 have begun only recently by knocking out genes richly expressed in CA2[20]. One suspected function of the new circuit is to regulate overlearning by the classical trisynaptic circuit[15, 20]. In this hypothetical regulation, the mutually inhibitory CA3→CA2 and CA2→CA3 connections where the two trisynaptic circuits intersect may play a crucial role. On the other hand, the direct ECIII input dedicated to CA1 has been implicated in temporal association memory[33], and this input may also underlie encoding of the temporal order of events in an episode[50]. The cell type-specific Cre

transgenic mice and optogenetics described in this study promise to be highly useful in testing these and other hypotheses at the behavioral level.

Methods

Methods are available in the online version of the paper.

Supplementary Material

Refer to Web version on PubMed Central for supplementary material.

Acknowledgments

We thank K. Rockland for helpful discussions, R. Neve for the generation of HSV, A. Burds for her support in the generation of the CA2 mouse line, A. Yoshii for helpful suggestion on PSD95 staining K. Fuji and A. Murakami for their support in the generation of the DG mouse line, C. Lovett, Y. Wang, W. Yu, L. Sultzman, N. Nayyar, M. Serock, C. Ragion, and H. Sullivan for technical support, T. Ryan, J. Z. Young and C. Yokoyama for comments on the manuscript. This work was supported by NIH grants R01-MH078821 and P50-MH58880 to S.T. and by Japanese Society for Promotion of Science to K.K..

References

1. Bird CM, Burgess N. The hippocampus and memory: insights from spatial processing. Nat Rev Neurosci. 2008; 9:182–194. [PubMed: 18270514]
2. Cajal, SRy. Histology of the nervous system of man and vertebrates. Oxford University Press; USA: 1995.
3. Marr D. Simple memory: a theory for archicortex. Phil Trans R Soc B Sci. 1971; 262:23–81.
4. Nakazawa K, Quirk MC, Chitwood RA, Watanabe M, Yeckel MF, Sun LD, Kato A, Carr CA, Johnston D, Wilson MA, Tonegawa S. Requirement for hippocampal CA3 NMDA receptors in associative memory recall. Science. 2002; 297:211–218. [PubMed: 12040087]
5. McHugh TJ, Jones MW, Quinn JJ, Balthasar N, Coppari R, Elmquist JK, Lowell BB, Fanselow MS, Wilson MA, Tonegawa S. Dentate gyrus NMDA receptors mediate rapid pattern separation in the hippocampal network. Science. 2007; 317:94–99. [PubMed: 17556551]
6. Nakashiba T, Young JZ, McHugh TJ, Buhl DL, Tonegawa S. Transgenic inhibition of synaptic transmission reveals role of CA3 output in hippocampal learning. Science. 2008; 319:1260–1264. [PubMed: 18218862]
7. Nakashiba T, Cushman JD, Pelkey KA, Renaudineau S, Buhl DL, McHugh TJ, Barrera VR, Chittajallu R, Iwamoto KS, McBain CJ, Fanselow MS, Tonegawa S. Young Dentate Granule Cells Mediate Pattern Separation, whereas Old Granule Cells Facilitate Pattern Completion. Cell. 2012; 149:188–201. [PubMed: 22365813]
8. de Nó RL. Studies on the structure of the cerebral cortex. II. Continuation of the study of the ammonic system. J Psychol Neurol (Lpz). 1934:113–177.
9. Andersen, P. The Hippocampus Book. Oxford University Press; USA: 2007.
10. Haglund L, Swanson LW, Köhler C. The projection of the supramammillary nucleus to the hippocampal formation: an immunohistochemical and anterograde transport study with the lectin PHA-L in the rat. J Comp Neurol. 1984; 229:171–185. [PubMed: 6501599]
11. Maglóczky Z, Acsády L, Freund TF. Principal cells are the postsynaptic targets of supramammillary afferents in the hippocampus of the rat. Hippocampus. 1994; 4:322–334. [PubMed: 7531093]
12. Bartesaghi R, Gessi T. Parallel activation of field CA2 and dentate gyrus by synaptically elicited perforant path volleys. Hippocampus. 2004; 14:948–963. [PubMed: 15390176]
13. Chevaleyre V, Siegelbaum SA. Strong CA2 Pyramidal Neuron Synapses Define a Powerful Disynaptic Cortico-Hippocampal Loop. Neuron. 2010; 66:560–572. [PubMed: 20510860]

14. Zhao M, Choi YS, Obrietan K, Dudek SM. Synaptic plasticity (and the lack thereof) in hippocampal CA2 neurons. J Neurosci. 2007; 27:12025–12032. [PubMed: 17978044]
15. Caruana DA, Alexander GM, Dudek SM. New insights into the regulation of synaptic plasticity from an unexpected place: Hippocampal area CA2. Learning & memory. 2012; 19:391–400. [PubMed: 22904370]
16. Piskorowski RA, Chevaleyre V. Synaptic integration by different dendritic compartments of hippocampal CA1 and CA2 pyramidal neurons. CMLS. 2012; 69:75–88. [PubMed: 21796451]
17. Jones MW, McHugh TJ. Updating hippocampal representations: CA2 joins the circuit. TINS. 2011; 34:526–535. [PubMed: 21880379]
18. Lein ES, Callaway EM, Albright TD, Gage FH. Redefining the boundaries of the hippocampal CA2 subfield in the mouse using gene expression and 3-dimensional reconstruction. J Comp Neurol. 2005; 485:1–10. [PubMed: 15776443]
19. Cui Z, Gerfen CR, Young WS. Hypothalamic and other connections with the dorsal CA2 area of the mouse hippocampus. J Comp Neurol. 2013; 521:1844–1866. [PubMed: 23172108]
20. Lee SE, Simons SB, Heldt SA, Zhao M, Schroeder JP, Vellano CP, Cowan DP, Ramineni S, Yates CK, Feng Y, Smith Y, Sweatt JD, Weinshenker D, Ressler KJ, Dudek SM, Hepler JR. RGS14 is a natural suppressor of both synaptic plasticity in CA2 neurons and hippocampal-based learning and memory. Proc Natl Acad Sci. 2010; 107:16994–16998. [PubMed: 20837545]
21. Shinohara Y, Hosoya A, Yahagi K, Ferecskó AS, Yaguchi K, Sík A, Itakura M, Takahashi M, Hirase H. Hippocampal CA3 and CA2 have distinct bilateral innervation patterns to CA1 in rodents. Eur J Neurosci. 2012; 35:702–710. [PubMed: 22339771]
22. Lein ES, et al. Genome-wide atlas of gene expression in the adult mouse brain. Nature. 2007; 445:168–176. [PubMed: 17151600]
23. Gonzales RB, DeLeon Galvan CJ, Rangel YM, Claiborne BJ. Distribution of thorny excrescences on CA3 pyramidal neurons in the rat hippocampus. J Comp Neurol. 2001; 430:357–368. [PubMed: 11169473]
24. Lein ES, Zhao X, Gage FH. Defining a molecular atlas of the hippocampus using DNA microarrays and high-throughput in situ hybridization. J Neurosci. 2004; 24:3879–3889. [PubMed: 15084669]
25. Wenzel HJ, Cole TB, Born DE, Schwartzkroin PA, Palmiter RD. Ultrastructural localization of zinc transporter-3 (ZnT-3) to synaptic vesicle membranes within mossy fiber boutons in the hippocampus of mouse and monkey. Proc Natl Acad Sci. 1997; 94:12676–12681. [PubMed: 9356509]
26. Swanson LW, Wyss JM, Cowan WM. An autoradiographic study of the organization of intrahippocampal association pathways in the rat. J Comp Neurol. 1978; 181:681–715. [PubMed: 690280]
27. Amaral DG, Witter MP. The three-dimensional organization of the hippocampal formation: a review of anatomical data. Neuroscience. 1989; 31:571–591. [PubMed: 2687721]
28. Sun GJ, Sailor KA, Mahmood QA, Chavali N, Christian KM, Song H, Ming G-l. Seamless reconstruction of intact adult-born neurons by serial end-block imaging reveals complex axonal guidance and development in the adult hippocampus. J Neurosci. 2013; 33:11400–11411. [PubMed: 23843512]
29. Zhang F, Wang LP, Boyden ES, Deisseroth K. Channelrhodopsin-2 and optical control of excitable cells. Nat Meth. 2006; 3:785–792.
30. Toni N, Laplagne DA, Zhao C, Lombardi G, Ribak CE, Gage FH, Schinder AF. Neurons born in the adult dentate gyrus form functional synapses with target cells. Nat Neurosci. 2008; 11:901–907. [PubMed: 18622400]
31. Mercer A, Trigg HL, Thomson AM. Characterization of neurons in the CA2 subfield of the adult rat hippocampus. J Neurosci. 2007; 27:7329–7338. [PubMed: 17611285]
32. Acsády L, Kamondi A, Sik A, Freund T, Buzsaki G. GABAergic cells are the major postsynaptic targets of mossy fibers in the rat hippocampus. J Neurosci. 1998; 18:3386–3403. [PubMed: 9547246]

33. Suh J, Rivest AJ, Nakashiba T, Tominaga T, Tonegawa S. Entorhinal Cortex Layer III Input to the Hippocampus Is Crucial for Temporal Association Memory. Science. 2011; 334:1415–1420. [PubMed: 22052975]
34. Nishimura-Akiyoshi S, Niimi K, Nakashiba T, Itohara S. Axonal netrin-Gs transneuronally determine lamina-specific subdendritic segments. Proc Natl Acad Sci. 2007; 104:14801–14806. [PubMed: 17785411]
35. Tamamaki N, Nojyo Y. Projection of the entorhinal layer II neurons in the rat as revealed by intracellular pressure-injection of neurobiotin. Hippocampus. 1993; 3:471–480. [PubMed: 8269038]
36. Steward O, Scoville SA. Cells of origin of entorhinal cortical afferents to the hippocampus and fascia dentata of the rat. J Comp Neurol. 1976; 169:347–370. [PubMed: 972204]
37. Steward O. Topographic organization of the projections from the entorhinal area to the hippocampal formation of the rat. J Comp Neurol. 1976; 167:285–314. [PubMed: 1270625]
38. Wickersham IR, Lyon DC, Barnard RJO, Mori T, Finke S, Conzelmann KK, Young JAT, Callaway EM. Monosynaptic restriction of transsynaptic tracing from single, genetically targeted neurons. Neuron. 2007; 53:639–647. [PubMed: 17329205]
39. Tamamaki N, Abe K, Nojyo Y. Three-dimensional analysis of the whole axonal arbors originating from single CA2 pyramidal neurons in the rat hippocampus with the aid of a computer graphic technique. Brain res. 1988; 452:255–272. [PubMed: 3401733]
40. Dong HW, Swanson LW, Chen L, Fanselow MS, Toga AW. Genomic-anatomic evidence for distinct functional domains in hippocampal field CA1. Proc Natl Acad Sci. 2009; 106:11794–11799. [PubMed: 19561297]
41. Mizuseki K, Diba K, Pastalkova E, Buzsáki G. Hippocampal CA1 pyramidal cells form functionally distinct sublayers. Nat Neurosci. 2011; 14:1174–1181. [PubMed: 21822270]
42. Rollenhagen A, Lübke JHR. The mossy fiber bouton: the “common” or the “unique” synapse? Front Syn Neurosci. 2010; 2:2.
43. Cenquizca LA, Swanson LW. Spatial organization of direct hippocampal field CA1 axonal projections to the rest of the cerebral cortex. Brain Res Rev. 2007; 56:1–26. [PubMed: 17559940]
44. Bannister NJ, Larkman AU. Dendritic morphology of CA1 pyramidal neurones from the rat hippocampus: I. Branching patterns. J Comp Neurol. 1995; 360:150–160. [PubMed: 7499560]
45. Bannister NJ, Larkman AU. Dendritic morphology of CA1 pyramidal neurones from the rat hippocampus: II. Spine distributions. J Comp Neurol. 1995; 360:161–171. [PubMed: 7499561]
46. Ishizuka N, Cowan WM, Amaral DG. A quantitative analysis of the dendritic organization of pyramidal cells in the rat hippocampus. J Comp Neurol. 1995; 362:17–45. [PubMed: 8576427]
47. Melzer S, Michael M, Caputi A, Eliava M, Fuchs EC, Whittington MA, Monyer H. Long-range-projecting GABAergic neurons modulate inhibition in hippocampus and entorhinal cortex. Science. 2012; 335:1506–1510. [PubMed: 22442486]
48. Contractor A, Swanson GT, Sailer A, O’Gorman S, Heinemann SF. Identification of the kainate receptor subunits underlying modulation of excitatory synaptic transmission in the CA3 region of the hippocampus. J Neurosci. 2000; 20:8269–8278. [PubMed: 11069933]
49. Berzhanskaya J, Urban NN, Barrionuevo G. Electrophysiological and pharmacological characterization of the direct perforant path input to hippocampal area CA3. J Neurophysiol. 1998; 79:2111–2118. [PubMed: 9535972]
50. MacDonald CJ, Lepage KQ, Eden UT, Eichenbaum H. Hippocampal “time cells” bridge the gap in memory for discontiguous events. Neuron. 2011; 71:737–749. [PubMed: 21867888]

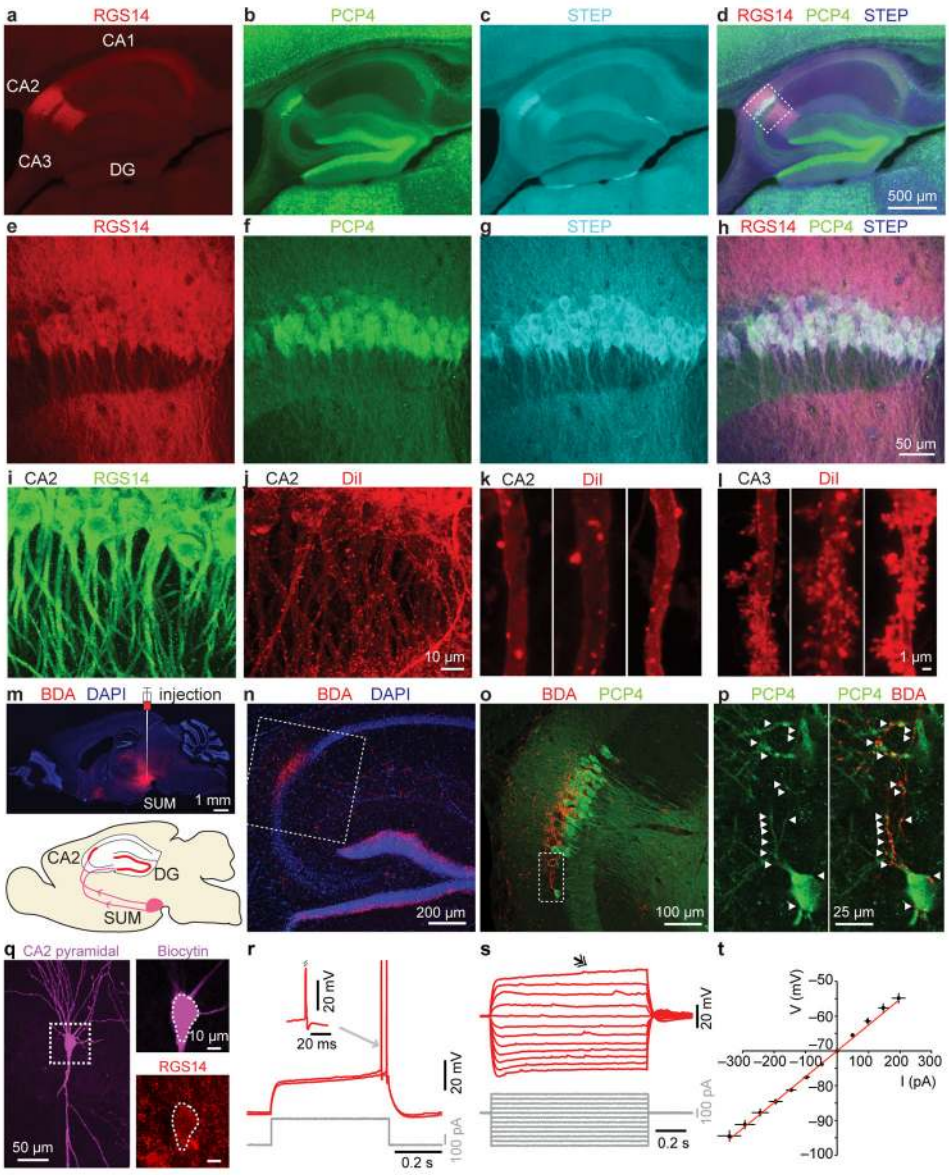

Figure 1. Molecular, cellular, anatomical, and electrophysiological definition of the CA2 region of the hippocampus

a–d, Representative images of the putative CA2 marker gene expressions, RGS14 (**a**), PCP4 (**b**), STEP (**c**), and a superposed image (**d**). **e–h**, Confocal images of CA2 from dotted line-box in (**d**). **i–j**, Zeta-projected confocal images of RGS14-positive CA2 neurons (**i**) and dendritic spine morphologies of CA2 neurons visualized by DiI (**j**). **k–l**, Typical dendritic morphologies of CA2 neurons showing a lack complex spines (**k**) and CA3 neurons with complex spines (**l**). **m–p**, Axonal dye tracer BDA was injected into the supramammillary nucleus (SUM). Injection site and diagram (bottom) showing axonal projections from SUM to CA2 and DG (**m**). Zeta-projected confocal image of BDA-positive terminals (**n**). Magnified image from the dotted line-box in (**n**) showing overlay between PCP4 and BDA (**o**). Single confocal stack from the dotted line-box in (**o**) showing overlay between PCP4-dendrites and BDA-positive terminals (**p**). **q**, Representative z-projected confocal image of a

biocytin stained CA2 pyramidal cell. Inset from the dotted-line box: single confocal stacks showing biocytin (top) and RGS14 staining (bottom). **r**, Patch-clamp recording from a CA2 pyramidal cell (same as **q**) in current clamp configuration showing the response to a positive step current injection. Note the late firing preceded by a slow depolarizing ramp. Inset: magnification of an action potential showing the fast hyperpolarizing potential. **s**, I–V curve, traces from the same cell in (**q**). Double arrowhead: note the slow depolarizing ramp. **t**, I–V for n=11 cells (mean±SEM), linear fit in red.

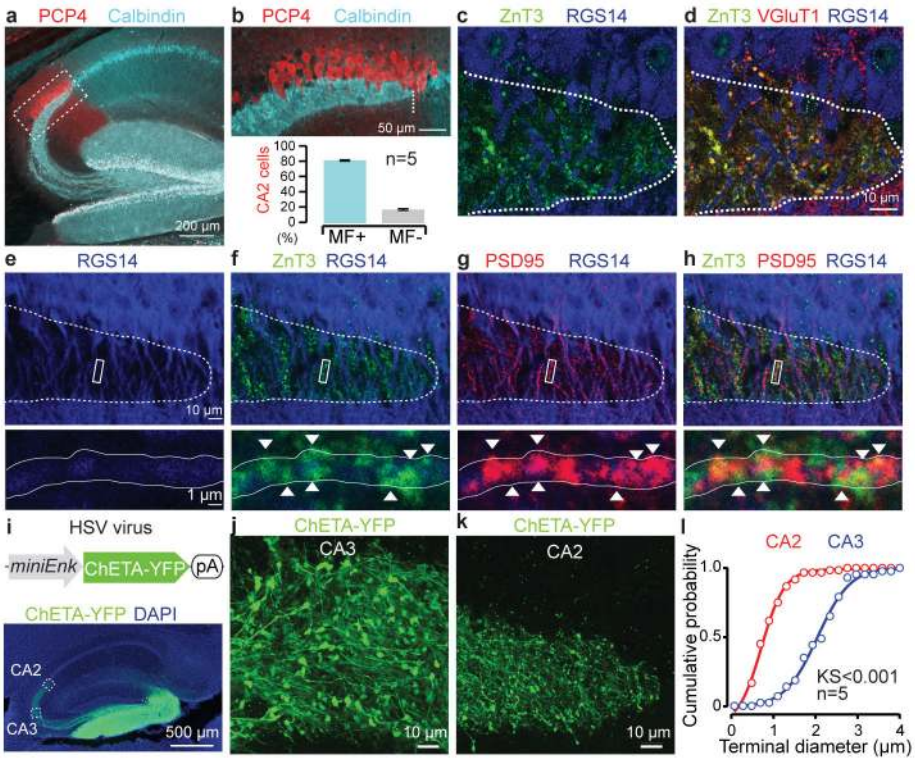

Figure 2. Dentate mossy fiber (MF) projections to CA2

a, Confocal image showing PCP4 and calbindin staining in CA2. **b,** Magnification (top) of dotted line-box in (**a**) and quantification (bottom) of the number of PCP4-positive CA2 cells receiving calbindin-positive MFs (MF+) and not receiving MFs (MF–). Data are represented as mean ± SEM. Dotted line indicates MFs ending point. **c**, Confocal image showing ZnT3 and RGS14 staining in CA2. **d**, Superposed image of ZnT3, VGluT1 and RGS14. Dotted lines in (**c**) and (**d**) enclose stratum lucidum. **e**, Confocal image showing RGS14-positive dendrites in CA2. **f**, Confocal image showing RGS14-positive dendrites and ZnT3-positive clusters. **g**, Confocal image showing RGS14-positive dendrites and PSD95-positive clusters. **h**, Superposed image showing ZnT3-PSD95 double-positive clusters on RGS14-positive dendrites. Bottom: magnification from the inset showing ZnT3-positive, PSD95-positive and ZnT3-PSD95 double-positive clusters (arrowheads). **i**, ChETA-YFP HSV construct (top). Confocal image of MFs visualized by ChETA-YFP (bottom). **i–k**, Z-projection from dotted line-boxes in (**e**) centered on CA3 (**j**) and CA2 (**k**). **l**, Cumulative histogram of MF terminal diameters for CA2 (n=60 boutons) and CA3 (n=43 boutons).

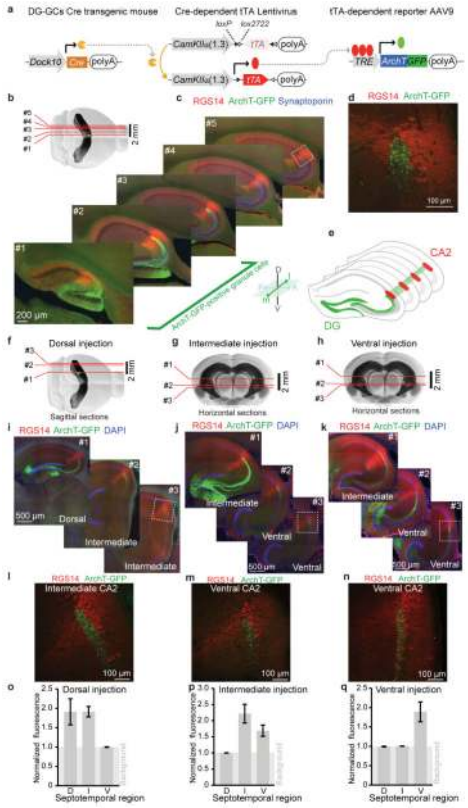

Figure 3. Longitudinal projections of Dentate mossy fibers (MFs) within CA2

a, Schematic of DGGC-specific transgenic Cre mouse, Cre-dependent tTA lentivirus and tTA-dependent ArchT-GFP-AAV9. Cre-recombinase switches on the expression of tTA in DGGCs inducing the expression of ArchT-GFP in DGGCs. **b**, Dorsorostral injection-site (green) and location of serial sections in (**c**). **c**, Serial images of RGS14, ArchT-GFP and synaptoporin (MF marker). DG cells in sections #1–3 express ArchT-GFP. **d**, Confocal image from the dotted line-box in (**c**). **e**, Longitudinal projections of MFs in CA2. **f–h**, Same approach applied to dorsal (**f**), intermediate (**g**) and ventral (**h**) DG injection sites (green dots) and location of serial sections in (**i**, **j**, **k**) respectively. **i–k**, Images showing extent and direction of MFs (green) within the RGS14-positive (red) CA2 region for dorsal (i), intermediate (**j**) and ventral (**k**) DG injection sites. **l–n**, Magnified confocal images from the corresponding dotted line-boxes in (**i, j, k**). **o–q**, Normalized fluorescence intesity of GFP-positive MFs terminals within dorsal (D), intermediate (I) and ventral (V) CA2, for dorsal (**o**), intermediate (**p**) and ventral (**q**) DG injection sites (n=6 samples per group from n=3 mice per injection site). Data are represented as mean ± SEM.

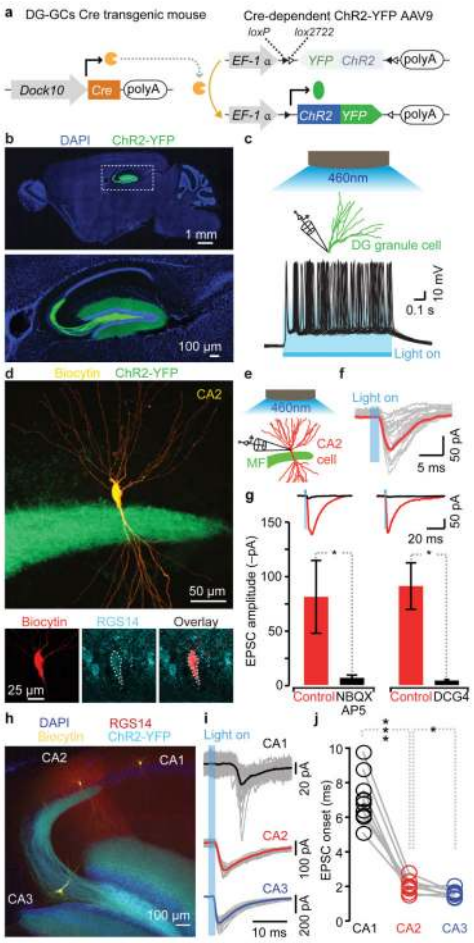

Figure 4. Functional monosynaptic connection of MF terminals onto CA2 pyramidal cells

a, DGGC-specific Cre transgenic mice were injected with Cre-dependent AAV9-EF1α-ChR2-YFP. Cre-recombinase switches on the expression of ChR2-YFP in DGGCs. **b**, DGGC-specific expression of ChR2-YFP (top) and enlarged image from the dotted line-box (bottom). **c**, Optogenetic stimulation of ChR2-YFP-positive DGGCs. **d**, Zeta-projected confocal image of a recorded CA2 pyramidal cell (yellow) overlapped by ChR2-YFP-positive MFs (green). Bottom: single confocal stacks showing colocalization of biocytin (red) and RGS14 (cyan). **e**, Patch-clamp recording of CA2 pyramidal cell and optogenetic stimulation of MFs in acute hippocampal slice. **f–g**, Optogenetic stimulation of MFs elicited an EPSC in a CA2 pyramidal cell (**f**) which is sensitive to NBQX/AP5 (n=5, two tailed paired t-test: **P*<0.05) and DCG-IV (n=5, two tailed paired t-test: **P*<0.05) (**g**). Data are represented as mean ± SEM. **h**, Representative zeta-projected confocal image of CA1, CA2 and CA3 pyramidal cells recorded in the same slice. **i–j**, EPSCs recorded in CA1, CA2 and CA3 pyramidal cells elicited by optogenetic stimulation of MFs (**i**). CA2 and CA3 cells displayed a fast EPSC onset whereas CA1 cells displayed a delayed onset (**j**, n=9 triplets, for CA1 and CA2, two tailed paired: t-test ****P*<0.001, for CA3 and CA2 **P*<0.05).

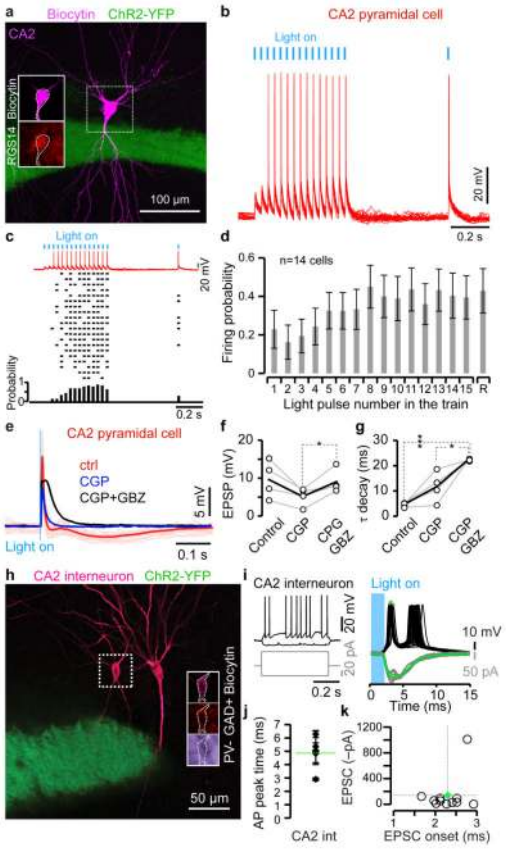

Figure 5. Response of CA2 cells to optogenetic stimulation of mossy fibers (MFs)

a, Z-projected confocal image of biocytin-filled CA2 pyramidal cell. Note ChR2-YFP-positive MFs. Inset from the dotted-line box: single confocal stacks showing biocytin (top) and RGS14 staining (bottom). **b**, Patch-clamp recording from a CA2 pyramidal cell (same as **a**) in current mode showing the spiking activity in response to optogenetic stimulation (30 Hz train) of MFs. **c**, Spiking activity of the same CA2 cell. Bottom: firing probability. **d**, Average firing probability in response to a 30 Hz train of light pulses for n=14 CA2 pyramidal cells. Note the increased probability in the recovery pulse R. **e**, Current clamp recording from a CA2 pyramidal cell in response to optogenetic stimulation of MFs showing a large EPSP (average of 30 traces in red) followed by inhibition sensitive to antagonists of GABAergic transmission (blue CPG, black GBZ). **f–g**, EPSP amplitude and decay, as shown in (**e**), are affected by GABAa and GABAb antagonists (two-tailed paired t-test: ***P<0.001, *P<0.05, n=4). Average: black lines. **h**, Z-projected confocal image of a biocytin-filled (violet) CA2 interneuron. Inset from the dotted line-box: CA2 interneuron GAD67-positive and parvalbumin-negative. Note the ChR2-YFP-positive MFs in green. **i**, Current (black) and voltage clamp recordings (green) of the same CA2 interneuron in (**h**), in response to optogenetic stimulation of MFs. Note the spiking activity (action potential peak time: green asterisks). Inset: intrinsic electrophysiological properties in response to current steps. **j**, First action potential peak times from n=5 CA2 interneurons in response to optogenetic stimulation of MFs (average: green dotted-line). **k**, EPSC amplitudes and onsets

from n=11 CA2 interneurons in response to optogenetic stimulation of MFs (average: green dot).

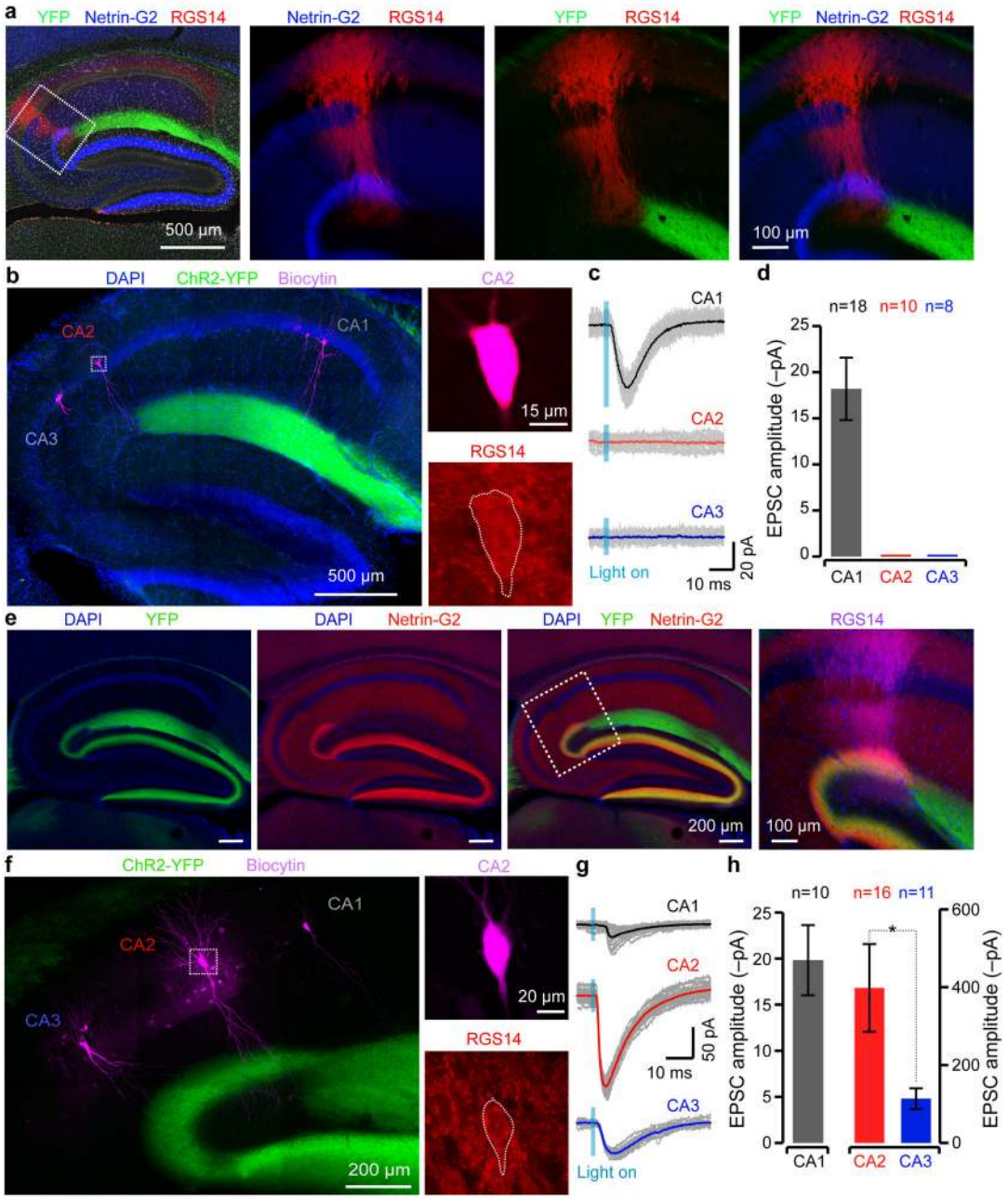

Figure 6. Cortico-hippocampal projections to CA2

a, The EC of a MECIII-specific Cre mouse was injected with a Cre-dependent AAV9-EF1α-ChR2-YFP. Parasagittal hippocampal slice stained for RGS14, netrin-G2 a MECII-specific marker and DAPI (white). On the side: enlarged confocal images from the dotted line-box. ChR2-YFP-positive MECIII fibers (green) are restricted to CA1-SLM and do not overlap with CA2. **b–d** Optogenetic stimulation of MECIII fibers. (**b**) Confocal image of biocytin-filled (violet) CA1, CA2, and CA3 pyramidal cells. Note ChR2-YFP-positive MECIII fibers (green) in CA1-SLM. Insets from the dotted-line box: CA2 pyramidal cell identified by colocalization of biocytin (violet) with RGS14 (red). (**c**) The same cells in

voltage clamp, in response to optogenetic stimulation of ChR2-YFP-positive MECIII fibers. (**d**) Only CA1 pyramidal cells displayed an excitatory response. **e**, The EC of a wild type mouse was injected with a non-Cre-dependent AAVrh8-CaMKIIα-ChR2-YFP. Parasagittal hippocampal slice expressing ChR2-YFP, stained for netrin-G2. On the side: enlarged images from the dotted line-box. YFP-positive MECII fibers costained with netrin-G2 (yellow) running into the DG, CA3 and overlapping with RGS14-positive dendrites of CA2. **f,** Confocal image of biocytin-filled (violet) CA1, CA2 and CA3 pyramidal cells. Note the ChR2-YFP-positive (green) MECII/III fibers. Inset from the dotted-line box: CA2 pyramidal cell identified by colocalization of biocytin (violet) with RGS14 (red). **g**, Same cells in voltage clamp, in response to optogenetic stimulation of ChR2-YFP-positive MECII/III fibers. **h**, Average EPSC amplitudes for CA1, CA2 and CA3 pyramidal cells. Data are represented as mean ± SEM.

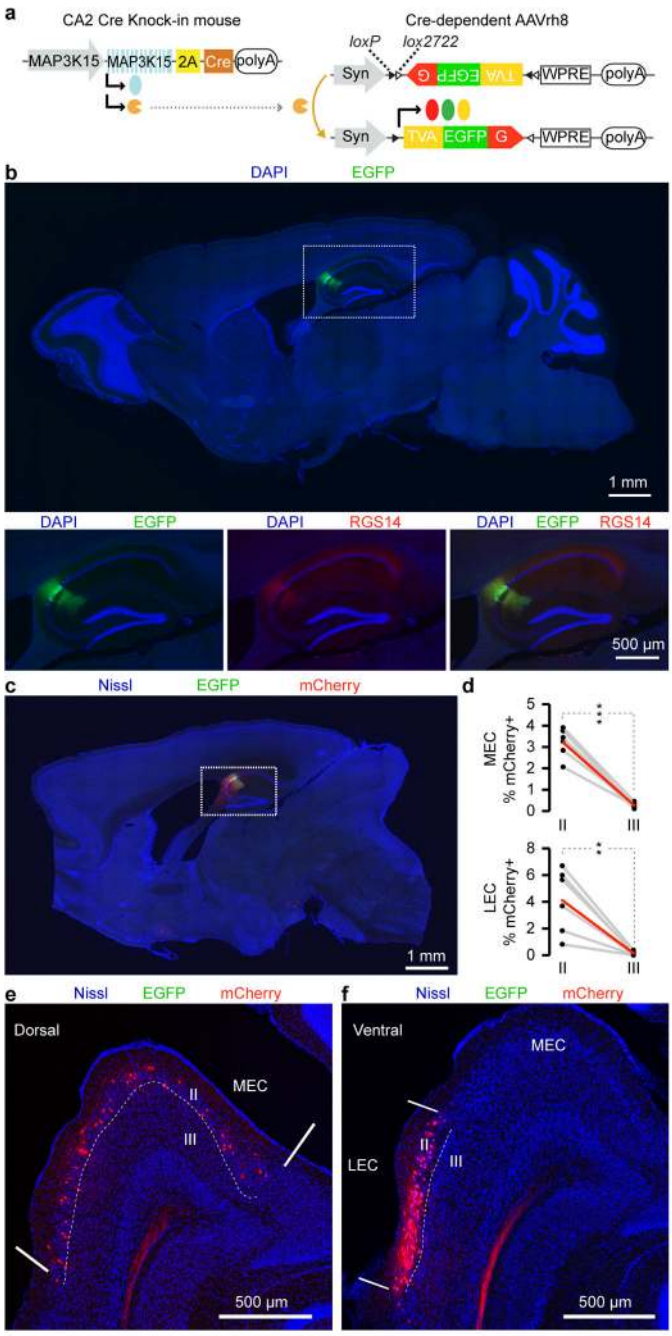

Figure 7. Mapping inputs to hippocampal CA2 neurons using the rabies virus-based monosynaptic tracing reveals MECII and LECII as the primary source of entorhinal inputs

a–b, Schematic (**a**) and sagittal whole brain section (**b**) from CA2-specific Cre mouse, injected with helper AAV. Insets from the dotted line-box: note the EGFP expression restricted to RGS14-positive CA2 pyramidal cells. **c**, Sagittal whole brain section from CA2-specific Cre mouse, injected with helper AAV and rabies virus (RV), expressing AAV-specific EGFP signal (green), RV-specific mCherry signal (red) and stained with Nissl (blue). **d**, Percent of mCherry-only positive cells in layer II and III of MEC (top) and LEC

(bottom), respectively (n=6 samples from 3 mice, two tailed paired t-test ***P<0.001 and **P<0.005, average in red). **e–f**, Horizontal sections showing the mCherry-only positive cells in both MEC (**d**) and LEC (**e**). Dotted line indicates ECII/ECIII border.

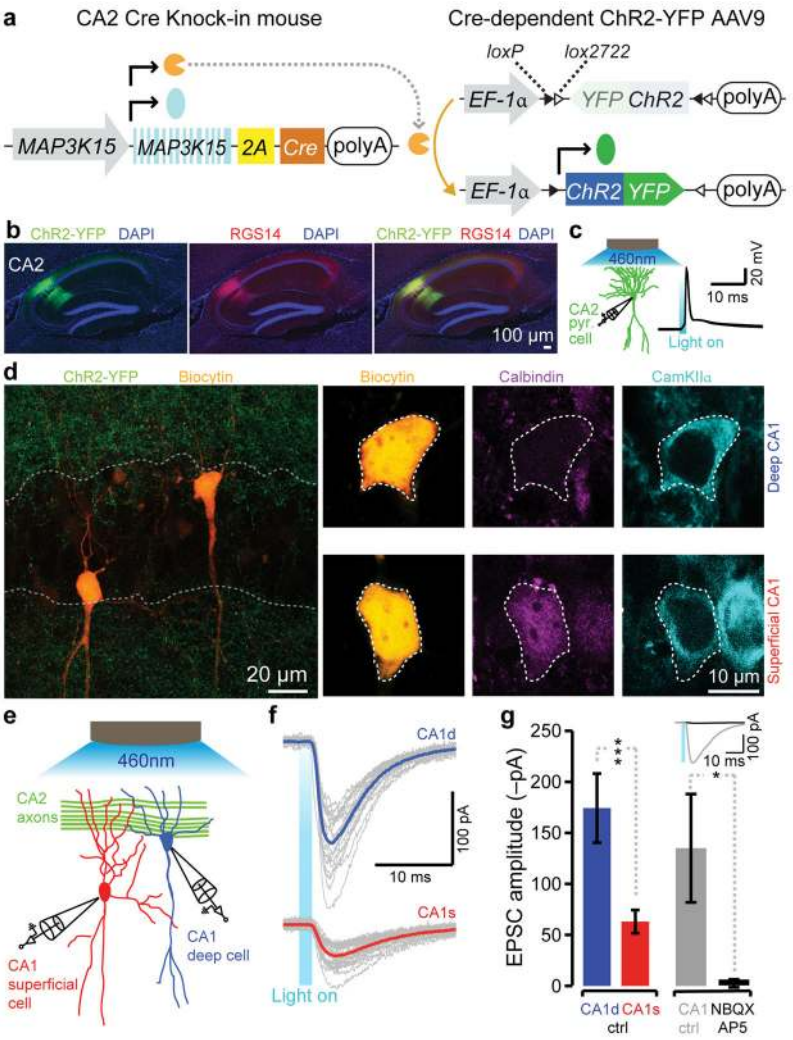

Figure 8. A preferential connection from CA2 to deep CA1 pyramidal cells establishes a novel trisynaptic circuit: DG-CA2-CA1$_{deep}$.

a, CA2-specific Cre knock-in mice were injected with Cre-dependent AAV9-EF1α-ChR2-YFP. Cre-recombinase switches on the expression of ChR2-YFP in CA2. **b**, ChR2-YFP expression in RGS14-positive CA2 cells. **c**, Optogenetic stimulation of a ChR2-YFP-positive CA2 pyramidal cell. **d**, Representative image of a recorded CA1 pyramidal cell pair located in different sublayers (dotted line: pyramidal cell layer). Upper side-panels: deep cell CaMKIIα-positive and calbindin-negative. Lower side-panels: superficial cell CaMKIIα-positive and calbindin-positive. **e**, Patch-clamp recordings of CA1 superficial and deep pyramidal cells combined with optogenetic stimulation of CA2 fibers in acute hippocampal slices. **f–g**, Optogenetic stimulation of CA2 fibers elicited EPSCs in a CA1 pyramidal cell pair. Deep pyramidal cells displayed a stronger response (n=14 pairs, two tailed paired t-test: ***P<0.001). EPSCs were sensitive to NBQX/AP5 (n=7, two tailed paired t-test: *P<0.05). Data are represented as mean ± SEM.